Acta Crystallographica Section F
Structural Biology and Crystallization Communications
ISSN 1744-3091

The *Corynebacterium glutamicum* aconitase repressor: scratching around for crystals

Javier García-Nafría,[a] Meike Baumgart,[b] Michael Bott,[b] Anthony J. Wilkinson[a] and Keith S. Wilson[a]*

[a]Structural Biology Laboratory, Department of Chemistry, University of York, York YO10 5DD, England, and [b]Institut für Biotechnologie 1, Forschungszentrum Jülich, 52425 Jülich, Germany

Correspondence e-mail: keith@ysbl.york.ac.uk

Received 17 June 2010
Accepted 20 July 2010

Imperfections on the surfaces of crystallization containers are known to influence crystal formation and are thought to do so by helping to overcome the nucleation barrier. The intentional creation of imperfections has been widely applied to induce crystallization of small molecules, but has not been reported for protein crystallization. Here, the crystallization and preliminary X-ray analysis of the TetR-type aconitase repressor are reported. This regulator was the first transcription factor to be identified in the regulation of the tricarboxylic acid cycle in *Corynebacterium glutamicum*, an organism that is of special industrial interest and is an emerging model organism for Corynebacterineae. Successful crystallization involved introducing manual scratches on the surface of standard commercial plates, which led to a substantial improvement in crystal nucleation and quality.

1. Introduction

Heterogeneous nucleation can be used to bypass the nucleation step in crystal formation (Saridakis & Chayen, 2009), which is separated from crystal growth by an entropic barrier. It is more than 20 years since the first epitaxial growth of protein crystals on minerals was observed (McPherson & Shlichta, 1988). Later studies involved the creation of charged surfaces (Falini *et al.*, 2002) and even surfaces to which the target protein was attached (Langmuir–Blodgett films) (Pechkova & Nicolini, 2002). The recent success of porous materials as heterogeneous nucleants has revitalized the field (Saridakis & Chayen, 2009) and many efforts are being directed to the application of this phenomenon (Kallio *et al.*, 2009). Recently, it was discovered that in addition to charged or porous materials, increased roughness and irregular surfaces can also induce nucleation (Liu *et al.*, 2007). Scratching a surface to promote crystal nucleation has been applied for many years in small-molecule crystallization, with crystals growing along the scratch. In contrast, even though crystals have been observed to grow from imperfections in surfaces or formed by imperfectly calibrated devices such as Mosquito robots, the application of intentional manual scratching has not been reported for the crystallization of proteins.

Corynebacterium glutamicum is a nonpathogenic predominantly aerobic Gram-positive soil bacterium that is widely used in industrial applications, especially in the production of amino acids such as L-lysine or L-glutamate (Hermann, 2003), and has recently become recognized as a model organism for Corynebacterineae, which include the human pathogens *Mycobacterium tuberculosis* and *C. diphtheriae*. Its Krebs cycle has recently been the subject of intensive studies because it is an important route for energy production and a source of precursors in the biosynthesis of amino acids of the aspartate and glutamate family (Bott, 2007). Aconitase (*acn*) catalyses the stereospecific isomerization of citrate into isocitrate *via cis*-aconitate in the tricarboxylic acid and glyoxylate cycles. It is also involved in the methylcitrate cycle, catalysing the conversion of methyl-*cis*-aconitate to methylisocitrate. Aconitase expression is regulated by a downstream-expressed transcription factor named the aconitase repressor (AcnR), which binds to a region upstream of the aconitase gene and was the first regulator to be found for the Krebs cycle in

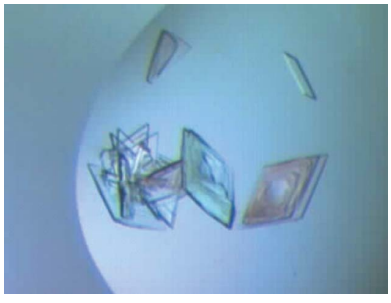

C. glutamicum (Krug *et al.*, 2005). Sequence comparisons show that AcnR belongs to the TetR superfamily of transcription factors, the members of which contain a helix–turn–helix DNA-binding motif in the N-terminal domain (Ramos *et al.*, 2005). AcnR is a homodimer in solution, with its dimerization being predicted to be mediated by its C-terminal regulatory domain. It is expected that the binding of AcnR to DNA and hence *acn* expression is controlled by the binding of a cofactor to the regulatory domain. However, no such ligand has been identified to date (Krug *et al.*, 2005).

In order to obtain a better understanding of the mode of action of AcnR and the *C. glutamicum* tricarboxylic acid cycle, we aim to determine its crystal structure. Here, we report how manually scratching the surface of 96-well MRC plates led to greatly improved nucleation and crystal growth of AcnR and improved crystal quality. To our knowledge, this is the first reported application of this approach in protein crystallography. We present a preliminary X-ray analysis together with heavy-atom derivatization.

2. Methods

2.1. Purification and crystallization

In brief, full-length AcnR (UniProt No. Q8NQ97) was over-expressed in *Escherichia coli* BL21 (DE3) using the plasmid pET-TEV-AcnR. A preculture of LB medium with 50 µg ml^{-1} kanamycin was inoculated from a fresh agar plate and grown with shaking (120 rev min^{-1}) at 310 K overnight. The cells were diluted 1:100 into fresh LB medium with kanamycin and grown with shaking (100 rev min^{-1}) at 310 K until they reached an OD_{600} of 0.4–0.6. Protein expression was induced by the addition of 0.5 m*M* isopropyl *β*-D-1-thiogalactopyranoside (IPTG). The cells were harvested after a further 4–6 h of cultivation at room temperature. Nickel-affinity chromatography was performed using a 1 ml HisTrap column (GE Healthcare, Munich, Germany) on an ÄKTA FPLC system (buffers used: equilibration buffer *A*, 100 m*M* Tris–HCl pH 8.0, 500 m*M* NaCl, 20 m*M* imidazole; buffer *B*, buffer *A* with 500 m*M* imidazole). The column was washed with 10%(*v*/*v*) buffer *B* and AcnR was eluted with a linear gradient to 100% buffer *B*. After nickel-affinity chromatography the N-terminal His tag was cleaved using TEV protease, yielding the full-length protein of 188 residues plus three additional amino acids, Gly, His and Met from the tag at the N-terminus. Gel filtration was performed using a HiLoad 16/60 Superdex 200 prep-grade column (GE Healthcare, Munich, Germany) as a final purification step to remove any aggregated protein (buffer: 20 m*M* Tris–HCl pH 7.5, 50 m*M* NaCl). The protein was flash-frozen in liquid nitrogen and stored in the gel-filtration buffer at 41 mg ml^{-1} at 193 K. The protein concentration was measured using absorbance at 280 nm assuming an extinction coefficient of 13 980 M^{-1} cm^{-1}. The sample was diluted in the same buffer to 16.5 mg ml^{-1} for initial crystallization screening using the commercial screens PACT (Molecular Dimensions), Index, Crystal Screen and Crystal Screen 2 (Hampton Research) in 96-well format with 150 + 150 nl drops in MRC plates using Hydra 96 (Robbins Scientific) and Mosquito (TTP LabTech Ltd, UK) robots. Plate-like crystals grew in clusters in condition No. 11 of Crystal Screen at 293 K. A crystal excised from this cluster (Fig. 1*a*) diffracted to 2 Å Bragg spacing in-house using a Rigaku MicroMax-007 HF rotating-anode source and a MAR 345 imaging-plate detector. However, the images showed diffraction from two or more lattices and it proved to be impossible to separate a single crystal from the cluster.

The crystals proved to be difficult to reproduce even with protein concentrations of up to 26.5 mg ml^{-1}. Several trays were set up with Crystal Screen condition No. 11, but most gave no crystals, until a second similar cluster was obtained in a single drop. This lack of reproducibility led us to investigate possible causes for the two successful hits. Two common factors emerged. Firstly, both clusters grew from small discontinuities in the shape of the drops at their edges (Figs. 1*a* and 1*b*). Secondly, the pH appeared to be critical. Condition No. 11 is reported to be 1 *M* ammonium phosphate,

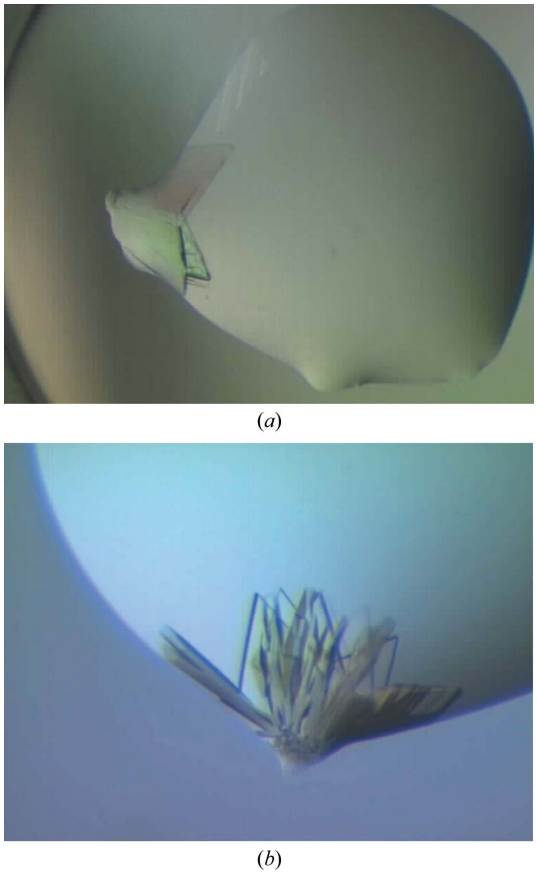

(*a*)

(*b*)

Figure 1
The initial clusters of AcnR crystals grown from Crystal Screen condition No. 11: 1 *M* ammonium phosphate, 0.1 *M* sodium citrate with a nominal pH of 5.6. (*a*) Initial plate-like clusters of crystals of roughly 100 µm in the longer dimension grow from small discontinuities at the edges of the drop. Diffraction of one of the plates showed reflections extending to 2 Å Bragg spacing and the presence of more than one crystal. (*b*) Plate-like cluster of crystals found in the same condition in a different tray growing from a discontinuity of the drop.

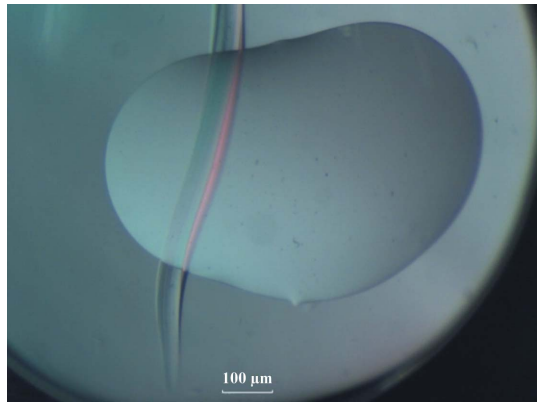

Figure 2
A typical scratch created with standard tweezers on the surface of a 96-well MRC sitting-drop plate. The scratch was made across the drop.

100 m*M* sodium citrate pH 5.6. However, the salt is not buffered and a rough estimation of the pH in the wells in the various trays using indicator paper suggested that the pH varied in the range 4–5. The two 'hit' drops both had a pH of ∼4, while drops with pH of ∼5 gave no crystals.

It was therefore decided to use freshly made Crystal Screen solution No. 11 for subsequent screens: for these the pH was indeed ∼4. In parallel, it was decided to introduce intentional deformations at the edge of the crystallization drops by making scratches (Fig. 2) on the surface of the 96-well MRC plates using standard tweezers, with the initial aim of forcing the drop to flow into the groove in order to simulate the environment seen in the deformations of the drop which had given the two clusters. This protocol led to the formation of large well defined crystals.

2.2. Heavy-atom derivatives

For a derivative search, the protein was diluted to 26.5 mg ml^{-1} and crystallizations were set up in 300 + 300 nl drops in 96-well MRC plates using a Mosquito robot, with the wells in the plates being scratched as described above. This provided over 100 crystals that were suitable for heavy-metal soaks. Three compounds were used at a range of concentrations, chloro(2,2′:6′,2″-terpyridine)platinum(II) chloride dehydrate at 1 m*M*, ethylmercury chloride at 2 and 4 m*M* and $K_2Au(CN)_2$ at 1, 2 and 4 m*M*, each with three different soaking times (2 h, 5 h and overnight), with several crystals in each of the conditions. After visual inspection, 60 crystals were judged to be suitable for diffraction experiments and were tested in-house using a Rigaku MicroMax-007 HF rotating-anode source, an R-AXIS IV++ imaging-plate detector and a Rigaku ACTOR system, which allows the automated mounting of samples. 15 crystals, including samples with all three heavy atoms, gave well ordered patterns and were selected for data collection with synchrotron radiation.

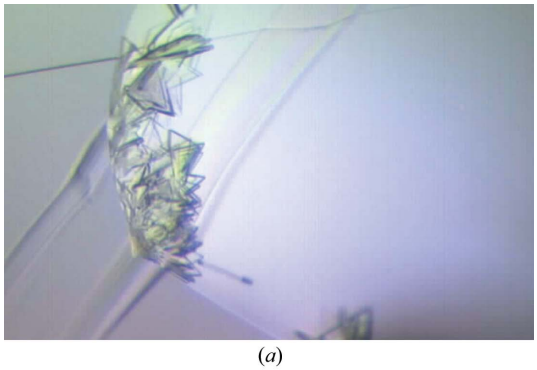

(*a*)

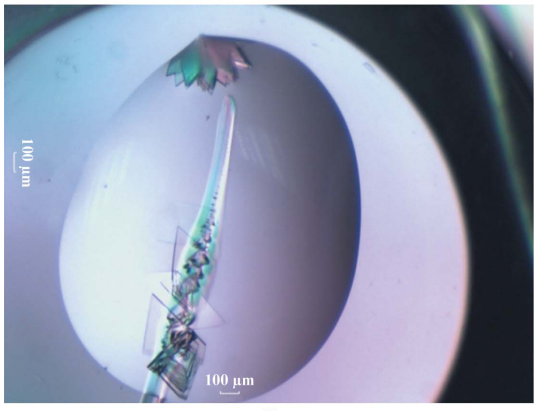

(*b*)

Figure 3
AcnR crystals growing from the scratches using Crystal Screen condition No. 11. (*a*) Crystals obtained from the discontinuities in the border of the drop created by manually introducing scratches in the wells. (*b*) Nucleation of crystals from such a scratch.

Table 1
X-ray data statistics.

Values in parentheses are for the outer resolution shell.

	AcnR native	AcnR Au SAD
Source	Diamond Light Source	ESRF
Beamline	I02	ID14-2
Wavelength (Å)	0.9795	0.9334
Data collection		
Space group	$P2_12_12_1$	$P2_12_12$
Unit-cell parameters (Å)	a = 34.21, b = 72.79, c = 145.57	a = 34.14, b = 72.88, c = 73.25
Resolution (Å)	1.65 (1.74–1.65)	2.54 (2.58–2.54)
Observed reflections	200330	175864
Unique reflections	44662	6461
R_{sym} or R_{merge}	0.082 (0.436)	0.073 (0.149)
$\langle I/\sigma(I)\rangle$	9.4 (2.7)	47.9 (21.9)
Completeness (%)	99.6 (99.2)	100 (100)
Redundancy	4.5 (4.5)	8.8 (8.4)

2.3. X-ray data collection and processing

Data were collected on beamline I02 at Diamond Light Source and on beamline ID14-1 at ESRF for the native protein and the heavy-atom derivatives, respectively. Crystals were mounted in a loop, flash-cooled and exposed to X-rays under a nitrogen stream at 100 K. For the native crystals, 600 images were collected with a 0.2° oscillation range and 0.5 s exposure time at a wavelength of 0.9795 Å. For the derivative crystals, 450 consecutive images were collected using an oscillation range of 0.5° and an exposure time of 0.5 s at a wavelength of 0.9334 Å. The native data were integrated and scaled with *iMOSFLM* (Leslie, 1999) and *SCALA*, while *HKL*-2000 (Otwinowski & Minor, 1997) was used for the derivatives. Data statistics are given in Table 1.

3. Results and discussion

From the initial screens, two clusters of plate-like crystals were obtained in Crystal Screen condition No. 11 (Fig. 1*a*). These crystals diffracted to 2 Å resolution, but it proved to be impossible to isolate a single crystal from either cluster. A lack of reproducibility led us to investigate the crystallization conditions in more depth and this led to the identification of the importance of (i) controlling the pH (at pH 4) and (ii) the presence of discontinuities at the edges of the drops where the clusters had grown. One explanation for the latter is that the small deformations contained a thinner liquid layer spread over a larger surface, causing faster evaporation; since the rate of evaporation also influences the kinetics of nucleation (García-Ruiz, 2003), this could provide appropriate local conditions to facilitate nucleation and growth.

Experiments were performed to investigate the effects of pH and nucleation. Firstly, to minimize any variation in pH, freshly prepared precipitant solutions with a pH close to 4 were used. Secondly, to determine whether discontinuities enhanced nucleation, scratches were made across the surfaces of the plates using standard tweezers (Fig. 2). As a control, identical drops were set up in adjacent wells without the introduction of scratches.

With the lowered pH, crystals now grew in many drops in both the scratched wells and the unscratched controls. However, there were marked differences in crystal quality and quantity between the

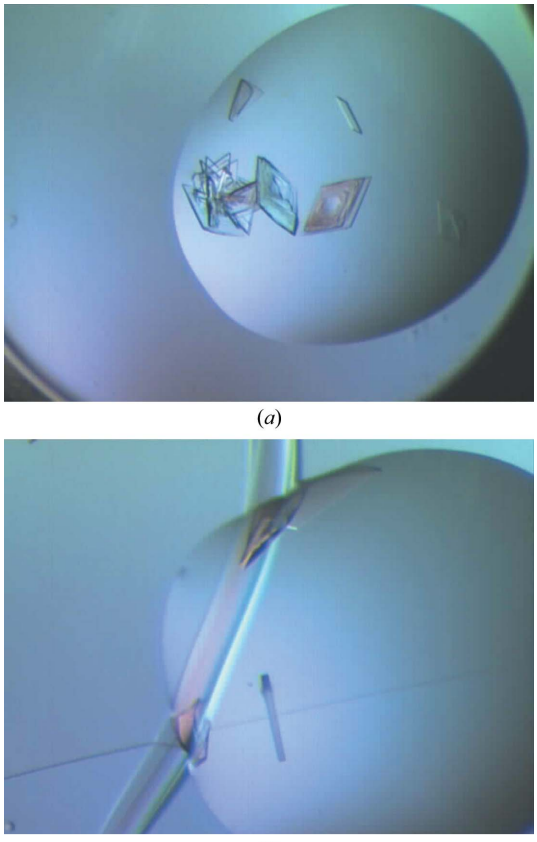

(*a*)

(*b*)

Figure 4
Comparison of crystals grown in scratched and scratch-free wells. (*a*) Crystals in scratch-free wells mainly form interpenetrating crystal clusters. (*b*) Crystals in a scratched well. Many grow along the side of the scratch, but a single crystal with well defined morphology can be seen suspended in the drop.

scratched and unscratched plates. The effects of the scratches were as follows.

Crystals grew from the distortions in the drops induced by the scratches (Fig. 3*a*), mimicking the effect observed at the discontinuities at the drop edges in the clusters obtained in the initial screens. This suggests that the scratches indeed provide different nucleation kinetics and that this considerably aids crystal nucleation. One explanation is that faster evaporation causes an increase in the speed of nucleation that is beneficial for crystal formation. A second possibility is that a higher concentration of the protein and precipitant may arise in these areas with a local faster evaporation of water. Alternatively, a combination of these factors may be responsible. In any case, the results demonstrate that changing the kinetics of the crystallization experiment can be beneficial, as has been suggested previously (Chayen & Saridakis, 2008).

In addition, the scratches often acted as more general nucleation points, with crystals growing in the middle and not just at the edges of the drops (Fig. 3*b*). The first heterogeneous nucleation was reported using minerals as nucleation points for crystal growth over 20 years ago (McPherson & Shlichta, 1988). Such heterogeneous nucleation bypassed the energy barrier for crystal nucleation, placing the experiment at the crystal-growth stage. Since then, many efforts have been directed towards finding a universal nucleation agent, testing a wide range of materials and strategies in order to overcome this bottleneck. Here, we have established that heterogeneous nucleation can occur at irregular surfaces, confirming previous observations (Liu *et al.*, 2007), and that manual scratches with standard laboratory tools can help in the nucleation of protein crystals. We are aware that success with this method is presently limited to a single protein and that the outcome is likely to be protein-dependent. However, the simplicity of the protocol suggests that it should be tested on a wider range of samples.

In addition, in more than half of the experiments better crystals, with no physical contact with the scratches, consistently grew in the scratched compared with the scratch-free wells. In these experiments, the scratch-free control drop did yield crystals but these were of lower quality, with extensive nucleation leading to interpenetrating crystals (Fig. 4*a*). In contrast, in the scratched well, while there was also extensive nucleation along the scratch, nicely separated single crystals grew in the rest of the drop (Fig. 4*b*).

Analysis of the resulting X-ray images for the native protein crystals revealed two crystal forms both belonging to Laue group *Pmmm*: $P2_12_12$, with unit-cell parameters a = 34.14, b = 72.88, c = 73.25 Å, and $P2_12_12_1$, with unit-cell parameters a = 34.21, b = 72.79, c = 145.57 Å. The unit-cell volumes in the two space groups differed by a doubling of the c unit-cell parameter in the second form. The V_M values of the two cells (2.16 and 2.15 Å^3 Da^{-1}, respectively) suggest that there is a single subunit of AcnR in the smaller unit cell and two independent subunits in the larger unit cell. This is in agreement with the presence of a noncrystallographic translation of 0.0, 0.043 and 0.5 in the larger cell based on analysis of the intensity data. The self-rotation function of the larger cell confirms that the only twofold axes are those generated by the crystal symmetry.

For the derivative crystals, two heavy-atom derivatives [from soaks with ethylmercury chloride and $K_2Au(CN)_2$] both in the smaller $P2_12_12$ crystal form gave data sets with significant anomalous signal, but only the crystal soaked in 2 m*M* $K_2Au(CN)_2$ overnight provided useful phase information. This is the first report of the crystallization of AcnR; structure solution is under way. The atomic structure of AcnR will provide insights into the regulation of the metabolic routes in which aconitase is involved.

We thank the European Commission for funding through the SPINE2-COMPLEXES project LSHG-CT-2006-031220. We thank Johan Turkenburg and Sam Hart for their assistance in data collection, and the staff at the ESRF (beamline ID14-1) and Diamond (beamline I02) for provision of synchrotron facilities.

References

Bott, M. (2007). *Trends Microbiol.* **15**, 417–425.
Chayen, N. E. & Saridakis, E. (2008). *Nature Methods*, **5**, 147–153.
Falini, G., Fermani, S., Conforti, G. & Ripamonti, A. (2002). *Acta Cryst.* D**58**, 1649–1652.
García-Ruiz, J. M. (2003). *J. Struct. Biol.* **142**, 22–31.
Hermann, T. (2003). *J. Biotechnol.* **104**, 155–172.
Kallio, J. M., Hakulinen, N., Kallio, J. P., Niemi, M. H., Kärkkäinen, S. & Rouvinen, J. (2009). *PloS One*, **4**, e4198.
Krug, A., Wendisch, V. F. & Bott, M. (2005). *J. Biol. Chem.* **280**, 585–595.
Leslie, A. G. W. (1999). *Acta Cryst.* D**55**, 1696–1702.
Liu, Y.-X., Wang, X.-J., Lu, J. & Ching, C.-B. (2007). *J. Phys. Chem. B*, **111**, 13971–13978.
McPherson, A. & Shlichta, P. (1988). *Science*, **239**, 385–387.
Otwinowski, Z. & Minor, W. (1997). *Methods Enzymol.* **276**, 307–326.
Pechkova, E. & Nicolini, C. (2002). *J. Cell. Biochem.* **85**, 243–251.
Ramos, J. L., Martínez-Bueno, M., Molina-Henares, A. J., Terán, W., Watanabe, K., Zhang, X., Gallegos, M. T., Brennan, R. & Tobes, R. (2005). *Microbiol. Mol. Biol. Rev.* **69**, 326–356.
Saridakis, E. & Chayen, N. E. (2009). *Trends Biotechnol.* **27**, 99–106.